A s ra

A novel planar robot is used to demonstrate that large numbers of axes are not required for effective manipulation, and that there can be strong advantages

A knowledgements

The work described in this dissertation is by f
ever worked on one set of problems. For a while, I
completion. On the other hand, I never was in mu
because CMU w

Contents

is Of Ta les

is Of Figures

Chapter 1

Introduction

The secret of getting ahead
is getting started.
Lucky Numbers 11, 16, 27, 28, 36, 37

have a higher-level programming language, in practice the two types of robots perform

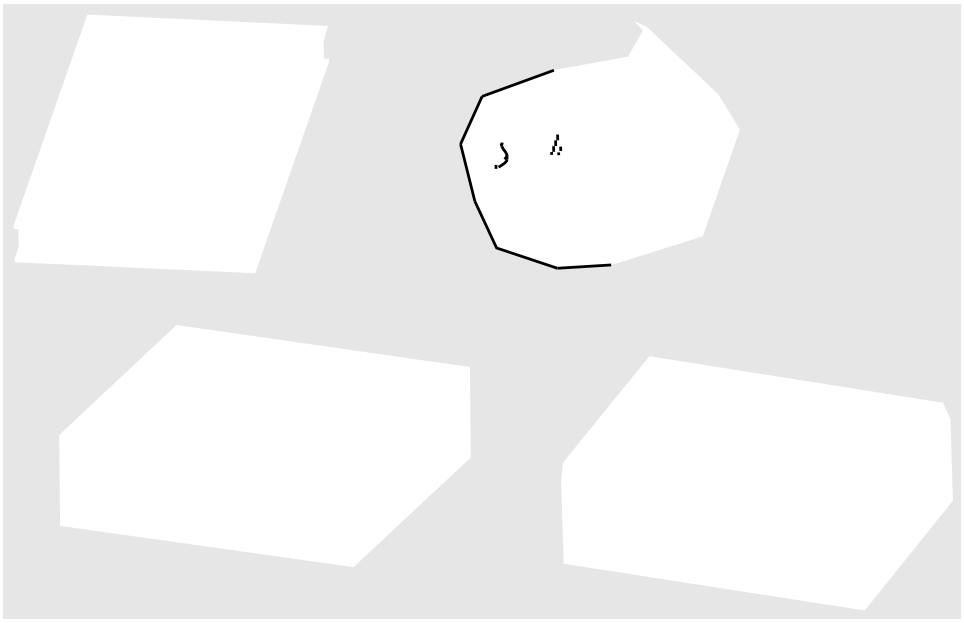

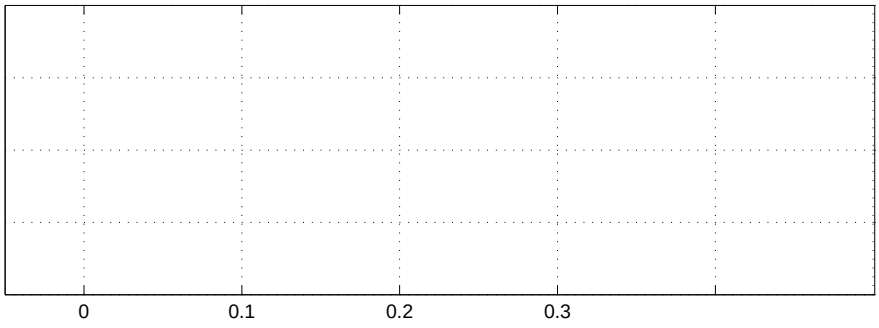
0
0.1
0.2
0.3

dimension	*normag0*	*normag1*, *normag2*, *vole*
d_f [mm]	96	150
d_a [mm]	24.5	48.5

0.3 μm (1σ). However, two of the four sensor segment output positions are averaged to compute the position of the forcer, which reduces the noise level to 0.2 μm ($1\ \sigma$) because the noise of each sensor is independent. The forcer skew angle is computed from the difference of either the x direction ($q_{\theta,x} = (p_{s1} - p_{s3})/d_s$) or y direction ($q_{\theta,y} = (p_{s2} - p_{s4})/d_s$) sensor segments divided by the distance bet ween sensors, d_s in Figure 1.8. In practice, both differences are computed and averaged to reduce

Contemporaneous with the RobotWorld introduction, a similar assembly workcell was designed at AT T [42] and Megamation, Incorporated[3] [43]. The Megamation systems differ from the RobotWorld systems in f o i T im o th a fu nt ion Thec nip

The IBM sensor was also used in work at Columbia University and Polytechnic University, including preliminary experiments with 1-DOF of a planar motor under PD control [26, 73], and modeling the actuator and sensing outputs as a function of skew angle [74]. Further work related to planar motors includes an investigation of the inaccuracies resulting from thermal deformations of the platen [75, 73], and a composite platen design for reducing eddy-current effects [76, 73]. A robust, adaptive controller was also designed for closed-loop control of a planar motor, but only simulation results have been reported [77, 78, 79, 80, 81, 82].

A capacitive sensing design was developed at Bell Laboratories [83, 84]. At MIT, several recent Master's Theses [85, 86, 87] have endied planar motor and sensor design, modeling, and control. They have reported experiments demonstrating 1-DOF sensor operation and PID control [88, 25]. Many researchers have been at g 1- cted to the problems of multiple tethered planar robots operating on a single platen [89, 90, 91, 92, 93]. Parallel mechanisms actuated by multiple planar robots have also been reported [94, 95, 73].

Most of the above work is focused on improving the g 1- jectory tracking and po-

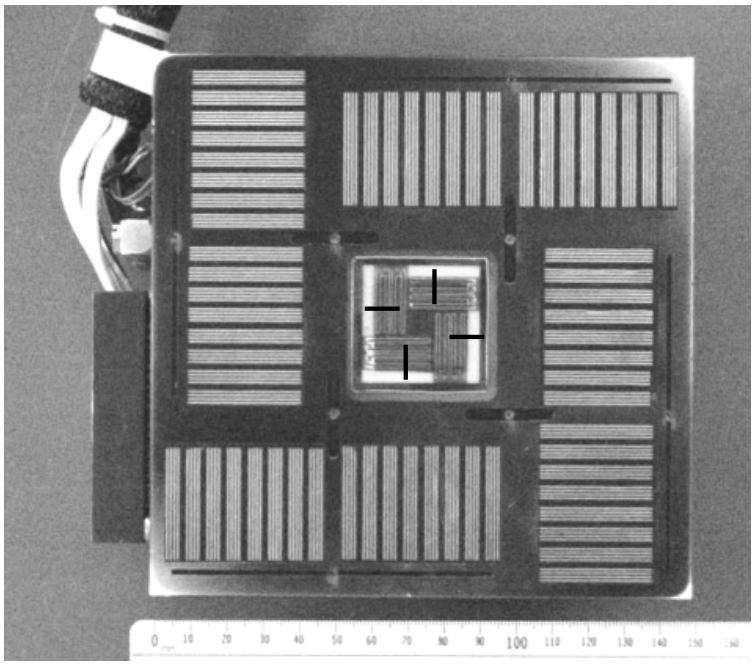

modifiable models to be used. How

w

forcers from different manufacturers may have variations in tooth geometry or mag-

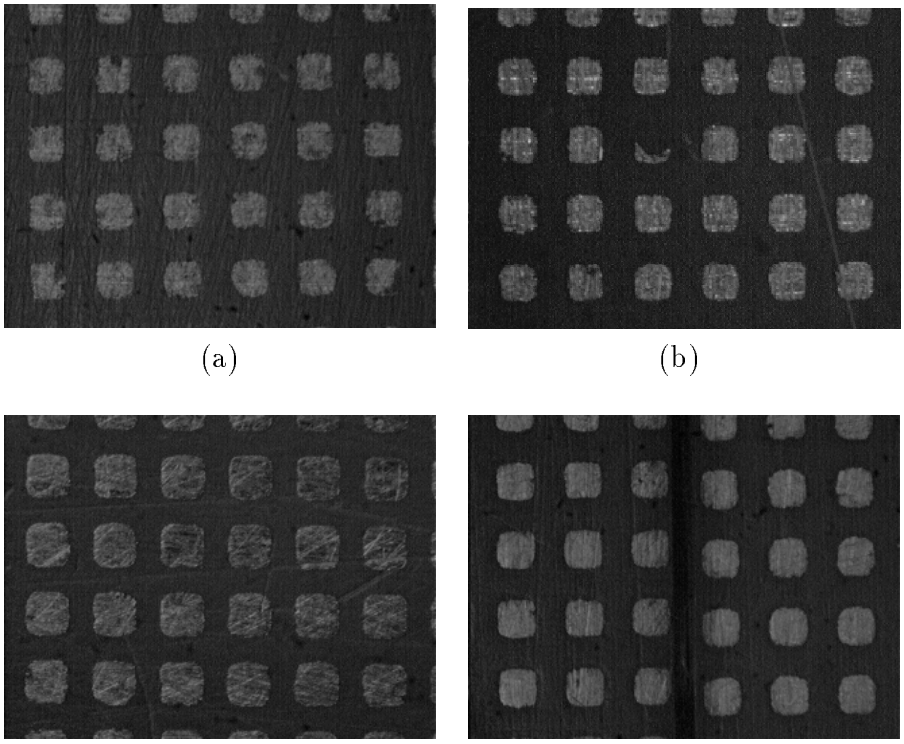

(a) (b)

(c) (d)

F

to skim this section for now

To provide a measurement of the courier position, a Zygo ZMI-1000 Interferometer system w

1.4.4 *v le* system

The *vole* system uses the planar robot body from the *normag1* system, with the Normag model 4XY1304-2-01 (serial number A10 forcer), integral platen sensor, and coordination sensor. However, the amplifiers and computing hardware are dramatically different. Eight Co iR model 4 212 amplifiers, a PowerPC motherboard, plumbing and controls for air and vacuum, and various custom printed circuit boards are integrated into a compact

1.4. Minifactory components

T e pla en diffe fro comm rc ae

Chapter 4

Communication

Each of the four linear motors in the forcer require two current inputs. In total, eight currents flow into the actuators, producing a net x, y force and a torque. The force generated by each motor is a function of its current values and its position and skew angle. A commonly-used first-order model for the force generated by a single motor

The last delay is from the commutation sample time, 1/3500 s for these tests, giving a total delay time of

$$\frac{1}{2} \cdot \frac{1}{3500} + 114 + 200$$

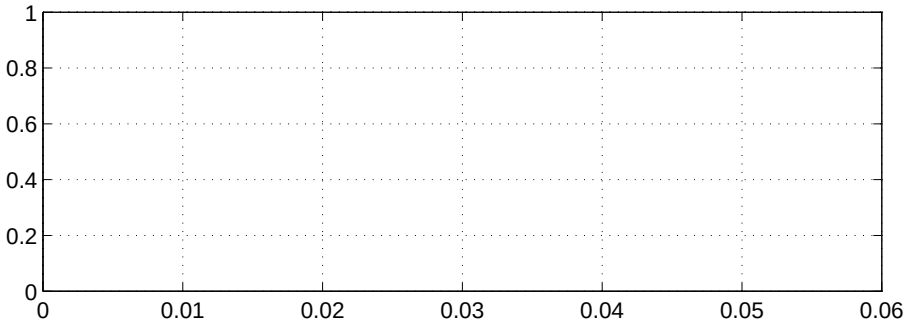
1
0.8
0.6
0.4
0.2
0
0
0.01
0.02
0.03
0.04
0.05
0.06

The importance of commutation is in simplifying the models that the controller must consider. With simpler models, simpler controllers can be used or additional higher-level goals can be integrated into the controller. Pushing higher-level goals down to lower levels permits the robot to react faster, improving its ability to dynam-

Chapter 3

Modeling

Dependent on the predictability and steadiness of life to support you!
Lucky Numbers 13, 14, 15, 24, 26, 34

With the commutator in place, actuator currents can be automatically selected by sending current commands to the commutator. However, recall that the force model used in Chapter 2 neglected second-order effects such as manufacturing errors, magnetic saturation, non-uniform teeth, imperfect amplifiers, finite update rates, and forcer rotations. The commutator also uses a static force model, neglecting

through a different area of the platen, or when the currents in the coils change, exerting different flux in one area of the platen. The currents act to resist the flux changes, and are dissipated by resistive losses in the platen. The net effect of eddy

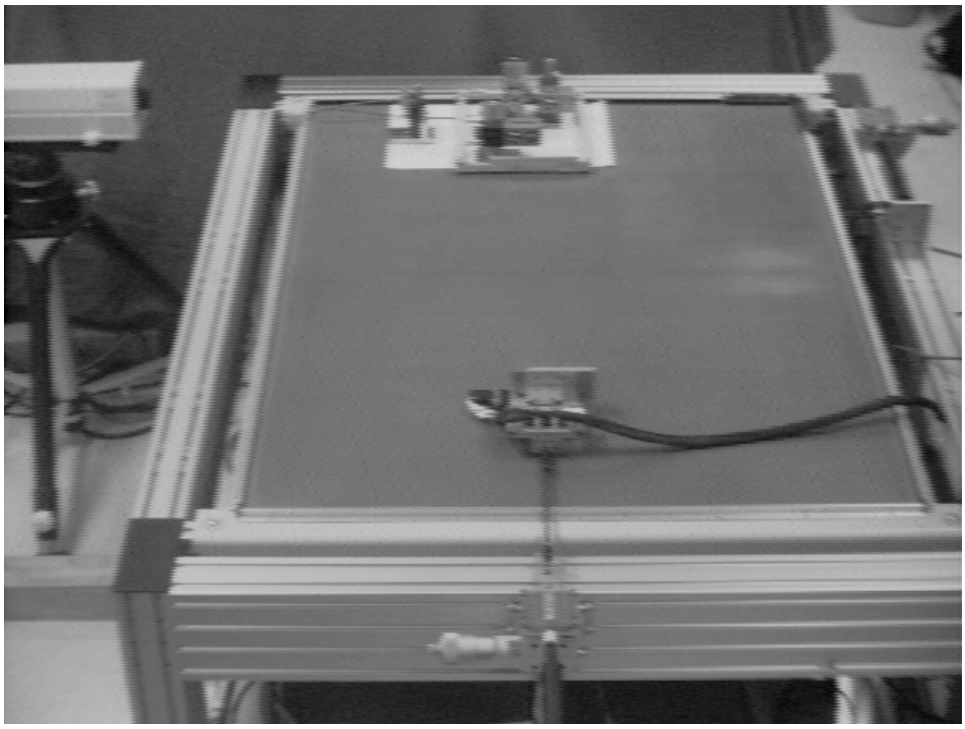

3.1 Static Force Characterization

In this section, the fidelity of the first-order force model (2.1),

$$f = k_A I_A \sin(\phi_a) + k_B I_B \cos(\phi_a), \tag{3.1}$$

with the coil currents reparameterized using (2.3)

$$I_A = I\cos(\psi_a) \quad \text{and} \quad I_B = -I\sin(\psi_a), \tag{3.2}$$

is investigated for cases where the motor velocity is near zero. Manufacturing imperfections in

decrease in k with increasing angle magnitude, and the phases ψ_a of the two motors

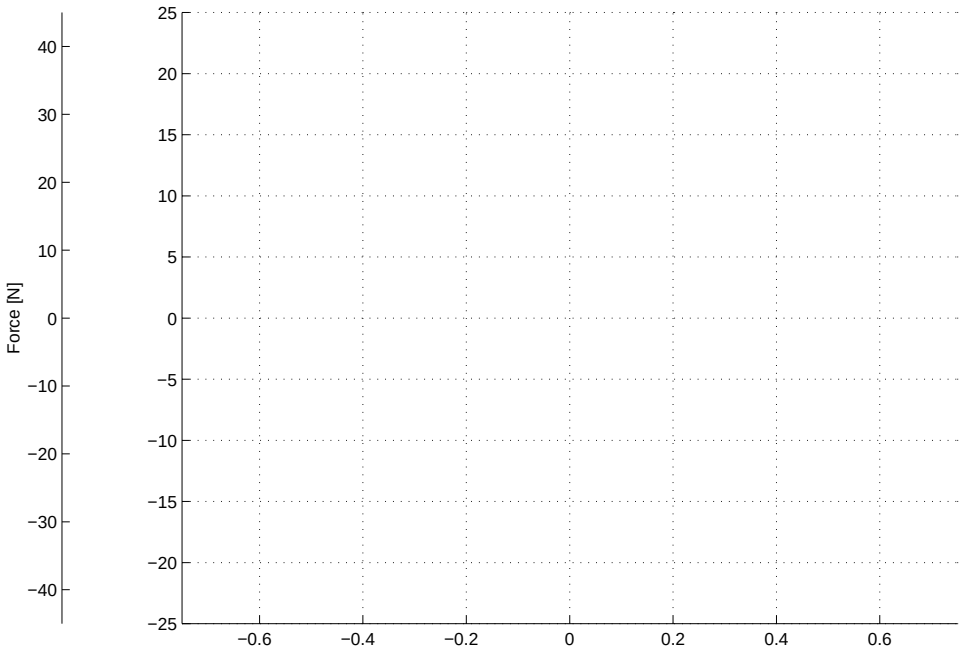
Force [N]
40
30
20
10
0
−10
−20
−30
−40
25
20
15
10
5
0
−5
−10
−15
−20
−25
−0.6
−0.4
−0.2
0
0.2
0.4
0.6

Neglecting static force effects which will tend to be averaged out at high velocities, the measured force f_m will be given by

$$f_m(v, f_c) = f_c + f_d(v, f_c) + f_r(v, f_c). \tag{3.12}$$

I

as a dashed line in Figure 3.7. It does not match the slope of our force computation except possibly near the zero velocity zone. However, this estimate supports the conclusion of a non-linear damping force, because if the dashed line is extended, it implies drastic drops in the available acceleration, which are not observed in the operation of the system.

Gjeltema [86], using a Normag motor, found the damping forces to be linear

to model the output delay in seconds caused by the amplifier assuming a forcer velocity of v m/s. Note that the velocity v is related to the phase fiot frequency, f_{amp} expressed in Hz, by $v = f_{amp}\mu$, and the delay t_{amp} is related to the phase amplitude ϕ_{amp} by $t_{amp} = \phi_{amp}/(360 f_{amp})$. The parameters k_1 and k_2 can then be optimized so that the delay time t_{amp} is lompatible with the data from the phase fiot of Figure 3. 9. For the *normag2* system, a least-squares fit produced parameter values $k_1 = 2.82 \times 10^{-5}$ s^2/ c2 6 and 8 (c 1 c 5 c ((c32e $\times$ 1

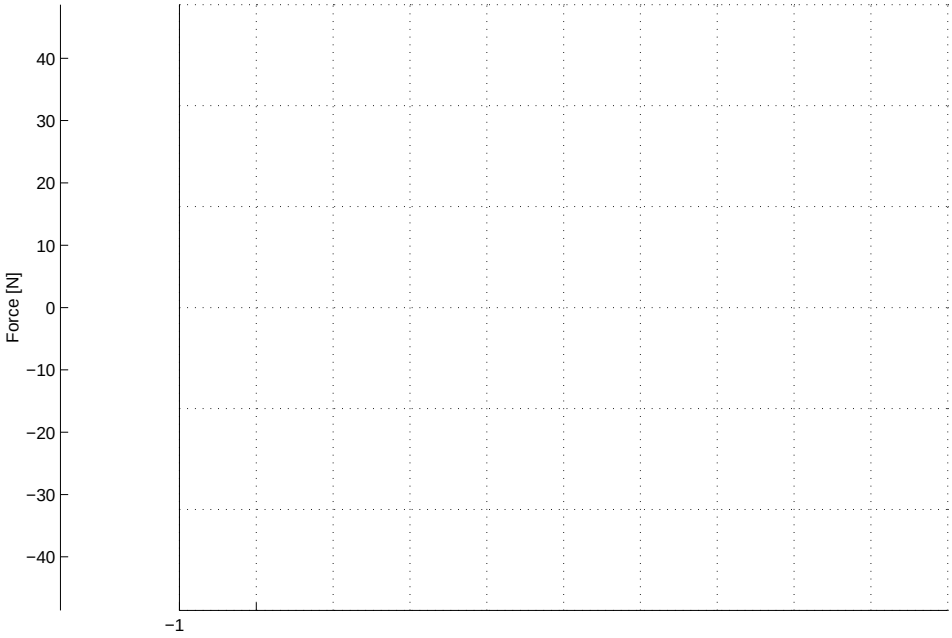
Force [N]
40
30
20
10
0
−10
−20
−30
−40
−1

Chapter 4

Autonomous Calibration

The measurements of the previous chapter can be used to construct detailed models for the force output of the linear motor actuators. These models would then be used in the commutator or controller to allow for more accurate force output. However,

to simultaneously calibrate the platen sensor parameters and the mounting parameters of the auxiliary *coordination sensor*. In Section 4.3, autonomous calibration of the actuator force outputs is presented. Finally, Section 4.4 presents details on the real-time implementation of the calibrated models.

4.1 Platen sensor autonomous calibration

4.1.1 Formulation

The platen sensor, mounted on the underside of the forcer, measures the location of forcer relative to the stationary platen teeth. Ideally, its quadrature decoding produces a perfect measure of the sensor's spatial phase. However, similar to the torque ripple of salient tooth actuators, the sensor will have spatial inaccuracies periodic in the tooth pitch. These inaccuracies will act as position-dependent disturbances that can lead to steady state errors and induce limit cycling in controllers with integral action. It is important to reduce these errors as much as possible. The sensor also relies on the locations of the platen teeth to determine motions beyond a single tooth pitch. There may be both long-range errors in the platen teeth [illegible]

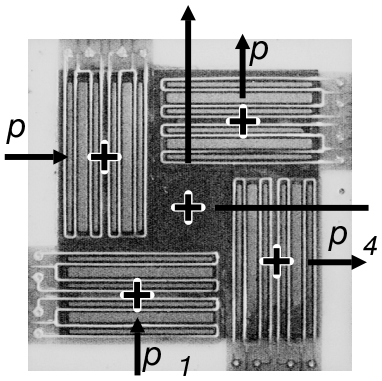

Figure 4.1: Platen sensor detail from *normag2* system

where $\check{p}_{s,i}$ is the uncalibrated output of the i^{th} sensor, $\omega_\rho := 2\pi/\mu$, μ is the pitch of the sensor teeth (1.016 mm for all devices in this document)

before and after calibration. The whole point of autonomous calibration is to elim-

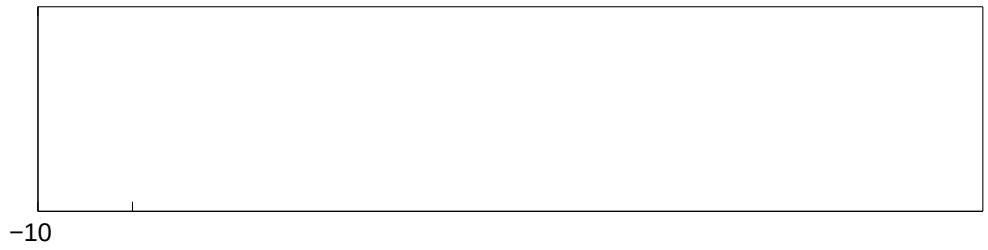
−10

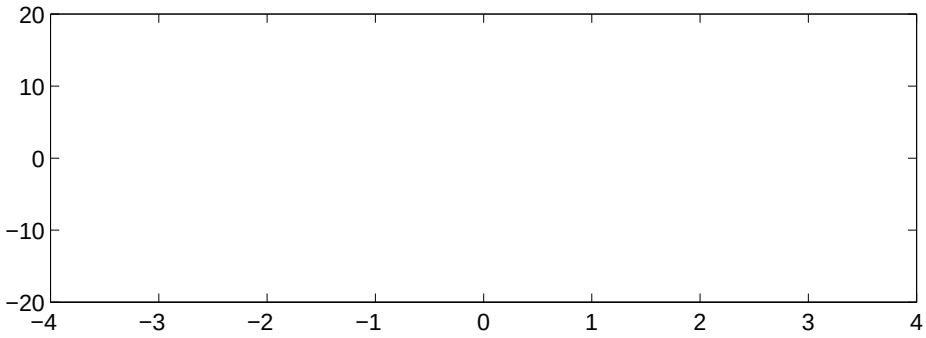
20
10
0
−10
−20
−4
−3
−2
−1
0
1
2
3
4

The laser interferometer was again sampled to provide an independent veri

allows the calibration of the full output r

However, if the current range is limited such that the linear term $k_{i,1}I_i$ dominates[5] the non-linear term $k_{i,2}I_i^3$, then the following linear model can instead be used

$$\begin{aligned} f_i \;:=\; \cos(k_\theta q_\theta)\{I_i(&k_{i,1} + k_{i,2}\sin(\omega_\rho p_{a_i}) + k_{i,3}\cos(\omega_\rho p_{a_i}) \\ &+ k_{i,4}\sin(2\omega_\rho p_{a_i}) + k_{i,5}\cos(2\omega_\rho p_{a_i}) \\ &+ k_{i,6}\sin(4\omega_\rho p_{a_i}) + k \qquad\qquad \cos(4\omega_\rho p_{a_i})) \\ &+ k_{i,8}\sin(\omega_\rho p_{a_i}) + k_{i,9}\cos(\omega_\rho p_{a_i}) \\ &+ k_{i,10}\sin(2\omega_\rho p_{a_i}) + k_{i,11}\cos(2\omega_\rho p_{a_i}) \\ &+ k_{i,12}\sin(4\omega_\rho p_{a_i}) + k_{i,13}\cos(4\omega_\rho p_{a_i})\}. \end{aligned} \tag{4.17}$$

It can be rewritten in linear form

$$f_i \;=\; \left[\right.$$

where d_a is the distance between actuators, as shown in Figure 1.8, and the output force d

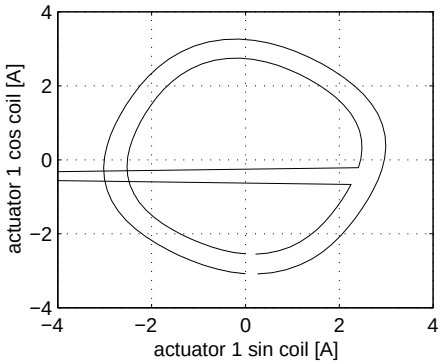
4
2
0
−2
−4
−4
−2
0
2
4
actuator 1 cos coil [A]
actuator 1 sin coil [A]

Parameter no.	k_0	$\hat{k}$
$k_{1,1}$	9.895	9.895
$k_{1,2}$	0.000	0.135
$k_{1,3}$	0.000	-0.181
$k_{1,4}$	0.000	-0.148
$k_{1,5}$	0.000	-0.239
$k_{1,6}$	0.000	0.192
$k_{1,7}$	0.000	-0.163
$k_{1,8}$	0.000	0.645
$k_{1,9}$	0.000	-1.410
$k_{1,10}$	0.000	-0.184
$k_{1,11}$	0.000	0.150
$k_{1,12}$	0.000	-0.213
$k_{1,13}$	0.000	-0.063
$k_{2,1}$	9.895	9.5000.000

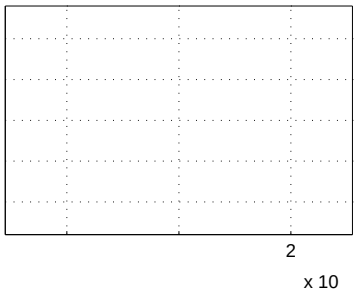
2
x 10

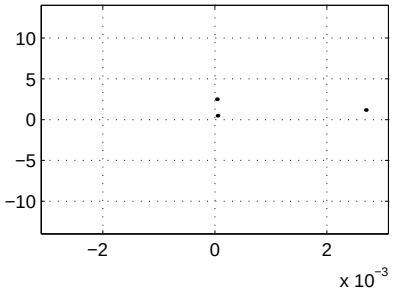
10
5
0
−5
−10
−2
0
2
x 10^−3

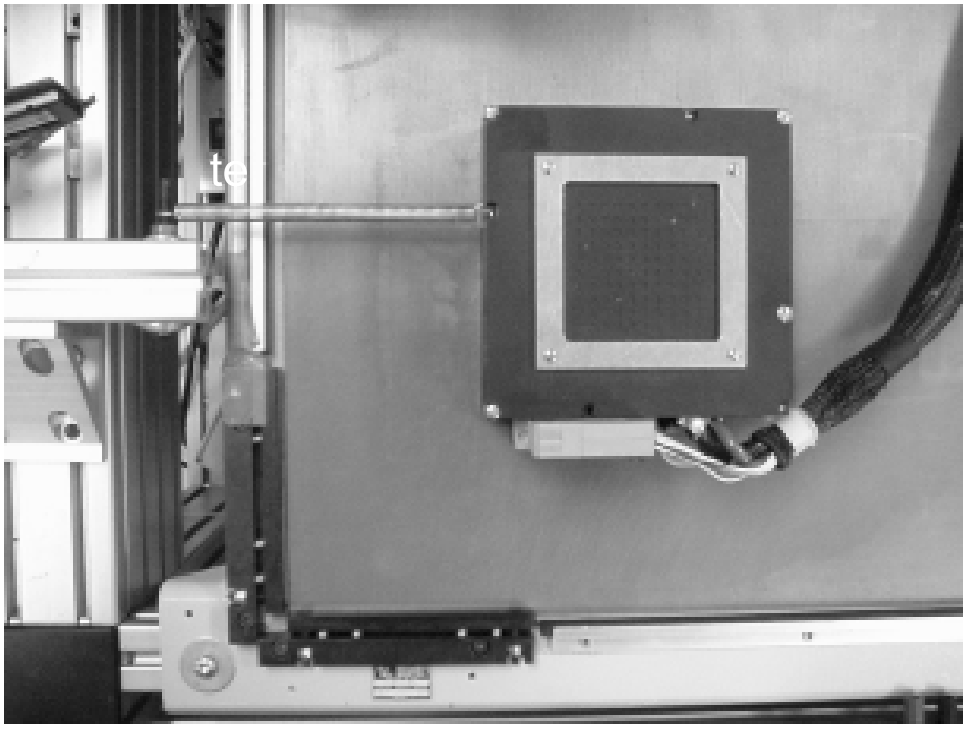

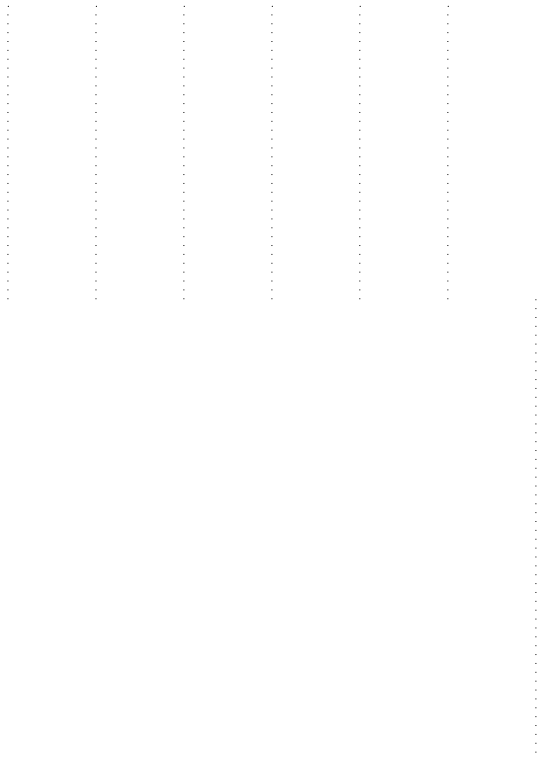

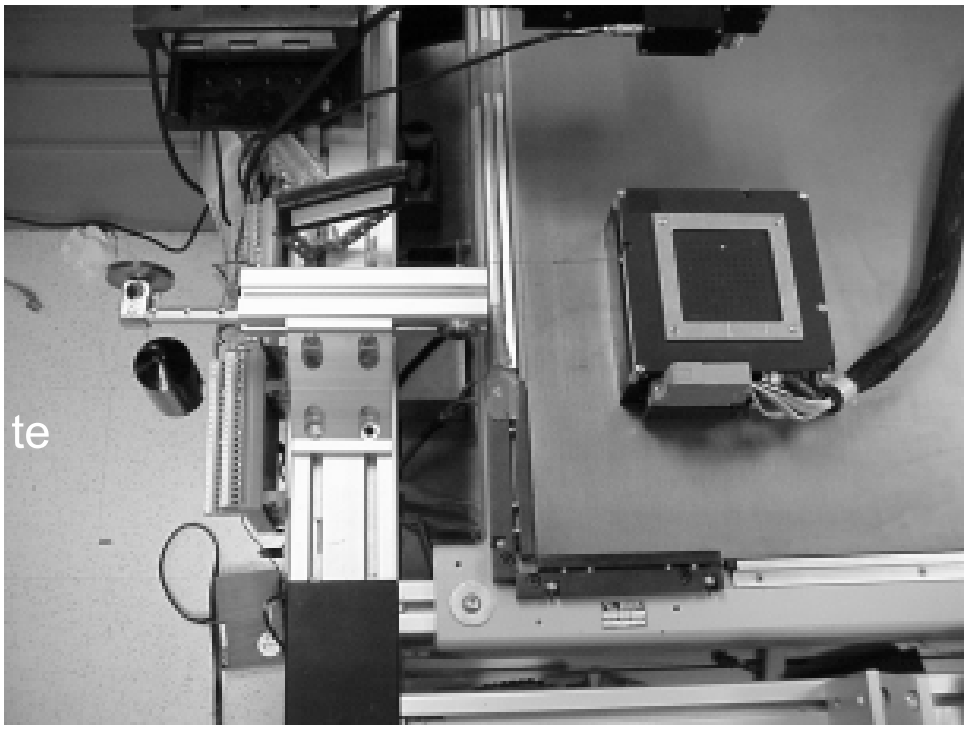
te

suspended, with the forcer moving to a sequence of positions under PID control. An integral term is used here to compensate for

Axis	mass [kg	Nominal	Calibrated	Improvement [%			
x	2.0	1.316	0.907	31			
x	1.5	1.229	0.879	28			
x	1.0	0.975	0.795	19			
x	0.5	0.945	0.768	19			
x	0.0	0.986	0.815	17			
y	2.0	2.740	1.700	38	1.5	1.930	1.005
				y	1.0	1.888	0.923
				y	0.5	2.028	1.258

Table 4.3

Pa
tion which takes les

the current to be useful to the commutator. Note that the force model (4.18) can be rewritten in the form

$$f_i = (a_{1,i}(p_{a_i}) + a_{2,i}(p_{a_i})u_i)\cos(k_\theta q_\theta) \ , \tag{4.28}$$

where $a_{1,i}(\cdot)$ collects the offset force terms and $a_{2,i}(\cdot)$ collects the current depende

C

fundamental frequencies at multiples of the robot speed, when measured in teeth per second. At rest, these errors can cause steady-state errors in the robot position

two pieces, as in Figure 1.12(d), or for the boundaries between the field-joinable platens used in the manufactory application presented in Chapter 7. In practice it is difficult to detect a malfunctioning sensor segment when crossing a platen discontinuity at high speed, so the locations of such discontinuities must be mapped ahead of time so that the appropriate sensor segments can be ignored while they are over a discontinuity. Note that when the sensor segment is [illegible]

The input to the force resolution function is the desired wrench $u_{w,ca}$, which may be outside, inside or on $\mathcal{F}$ leading to over-, under-, and uniquely-constrained cases.

In the under-constrained case, an infinite number of solutions for f can be found that will generate the desired wrench. Here, we choose the solution:

$$\begin{bmatrix} f_{x1} \end{bmatrix}$$

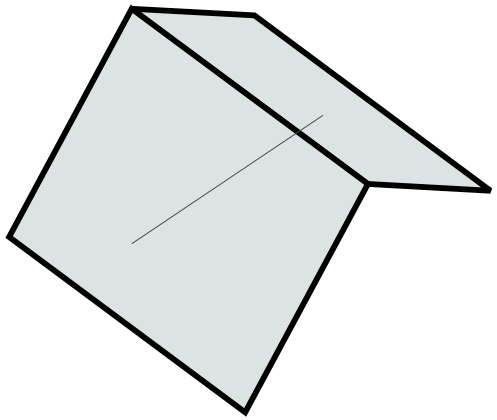

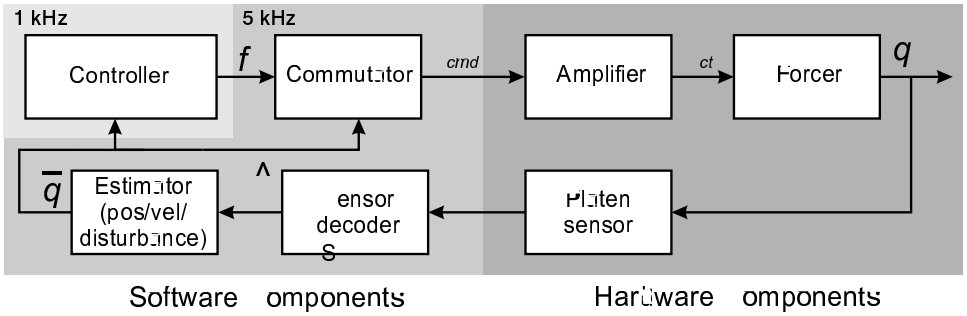

Figure 5.3: Restricted domain controller block diagram

.1.

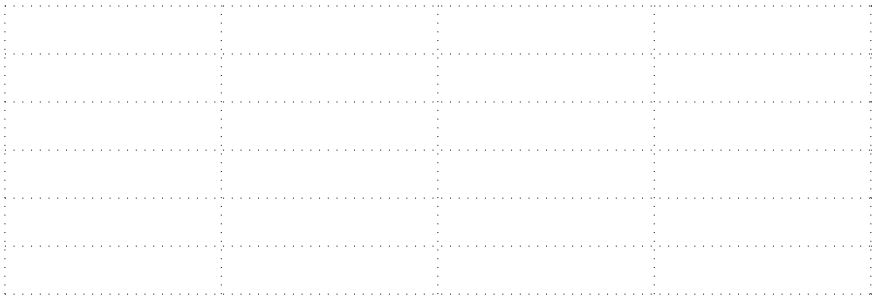

thermal effects. The crosses in Figure 5.5 show this bi-directional position repeatability for the PID controller to be under 2.5 μm peak-to-peak, and the skew angle repeatability to be under 0.02° peak-to-peak over 36 motions. Note that the error increases at a ravel distance of about 20 mm, which is when the linear motors start

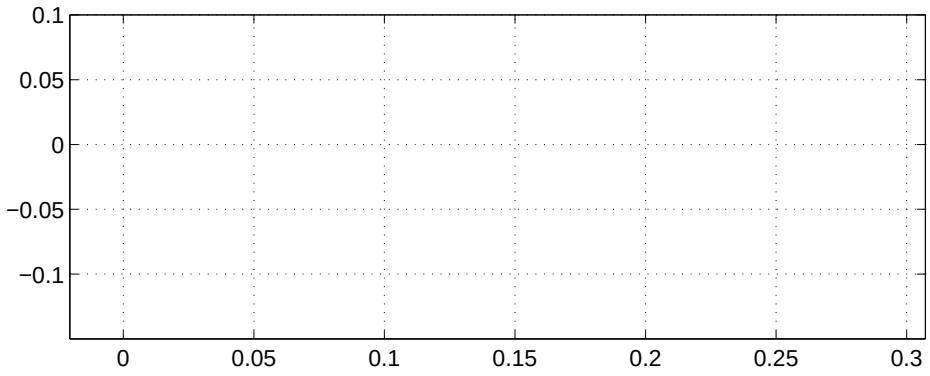
0.1
0.05
0
−0.05
−0.1
0
0.05
0.1
0.15
0.2
0.25
0.3

case, there will be a consta

from prior work [

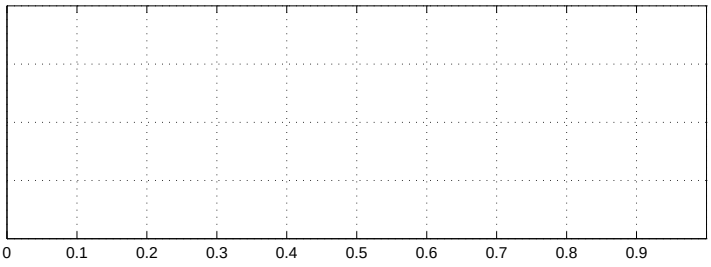
0
0.1
0.2
0.3
0.4
0.5
0.6
0.7
0.8
0.9

C

Recently, such *hybrid* control techniques have been used to move higher-level decisions into the controller in a provably stable manner. Time-varying system dynamics [116], constraints [117, 100], disturbances [118], and control level programming of dynamic tasks [119] have been incorporated into the framework of hybrid controllers.

The main complication for motion planning of planar robots arises when a single platen. In this case, a collision avoidance scheme [66]. The task considered in this chapter is the transportation overhead devices. The traditional approach would be to construct problem and choose a collision-free set of trajectories for the robots bances may make it impossible to track an aggressive time-parameterization and overshoot which could lead resulting in controller saturation problems because an exact spatial and temporal

requires careful consideration of the boundaries, while also efficiently bringing $\dot{q}$ to $\hat{v}(q)$. However, a *stop* contro

used in a regulation mode during robot motions, but the controller parameters are related to motion and velocity profiles that are not directly relevant. The angle inaccuracies are also a significant fraction of the rotational limits of the device, which caused the monotonicity of the controller sequencing to break. The controller would reach the goal, but the monotonicity of the controller sequences was violated due to the angular errors, resulting in some momentary chattering that slowed the prog

Chapter 7

Mimifactory

T

can be performed using the standard minifactory agents. It is not necessary to desi

An implication of dis

platen sensor is operational over a rotational range of severa

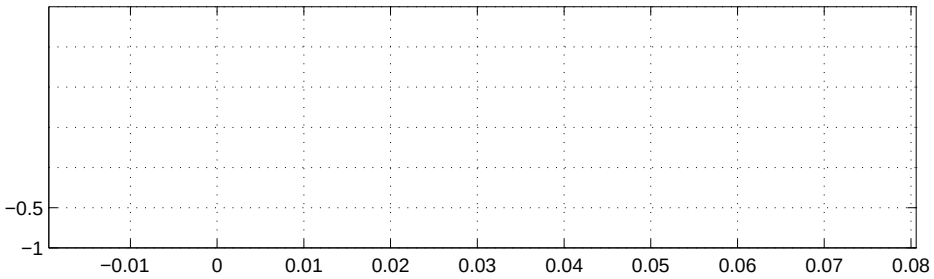
−0.5
−1
−0.01
0
0.01
0.02
0.03
0.04
0.05
0.06
0.07
0.08

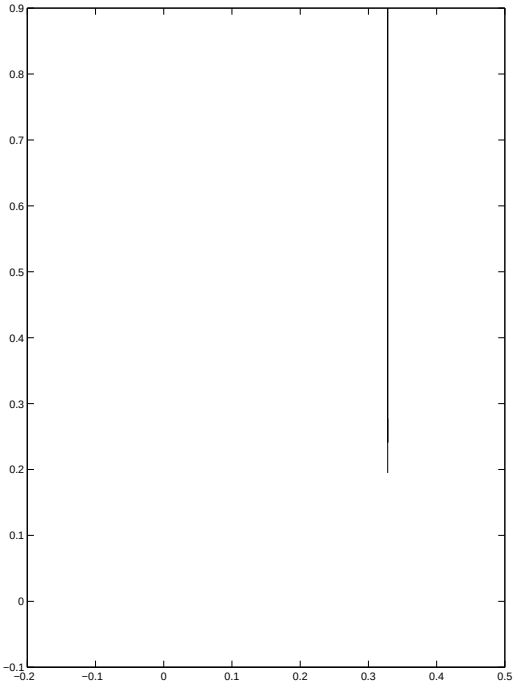
0.9
0.8
0.7
0.6
0.5
0.4
0.3
0.2
0.1
0
−0.1
−0.2
−0.1
0
0.1
0.2
0.3
0.4
0.5

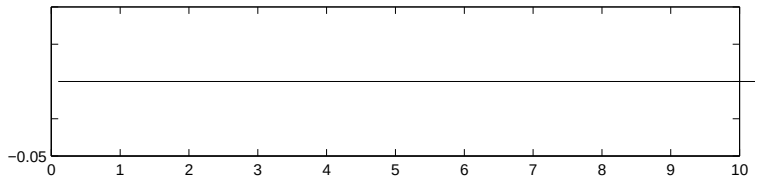
−0.05
0
1
2
3
4
5
6
7
8
9
10

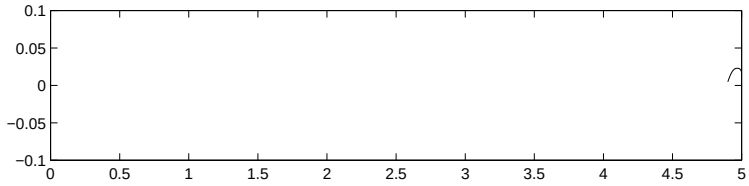
0.1
0.05
0
−0.05
−0.1
0
0.5
1
1.5
2
2.5
3
3.5
4
4.5
5

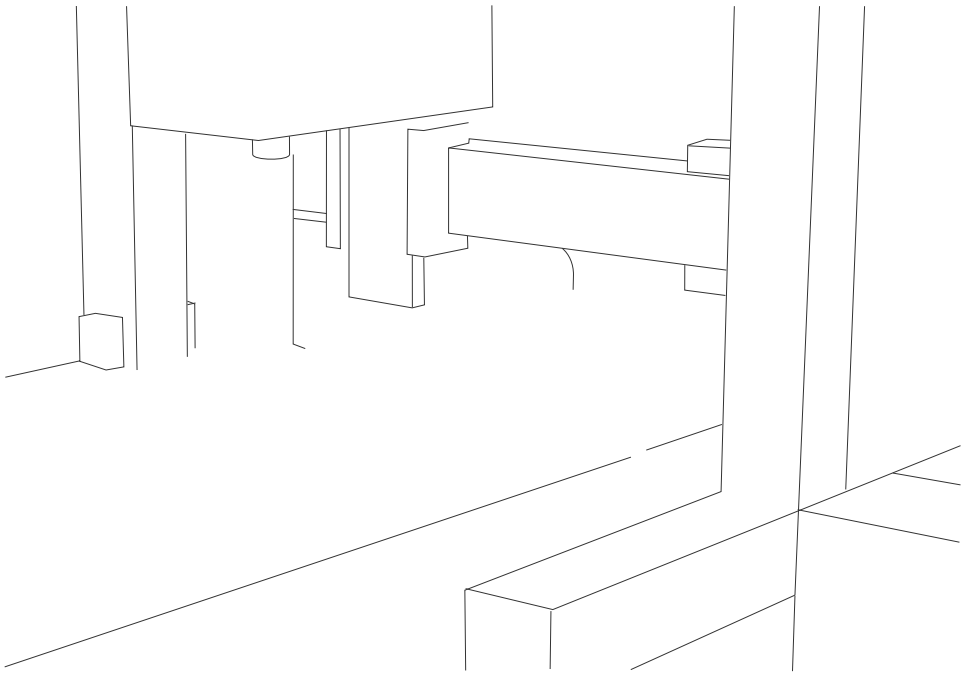

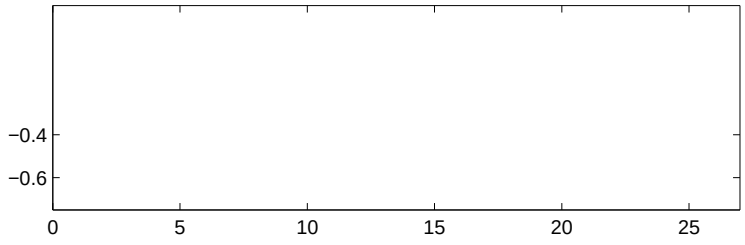
−0.4
−0.6
0
5
10
15
20
25

Starting from a re

C ap er 8

Appli a io : A imi ia ure o ile par s fee er

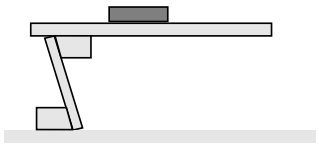

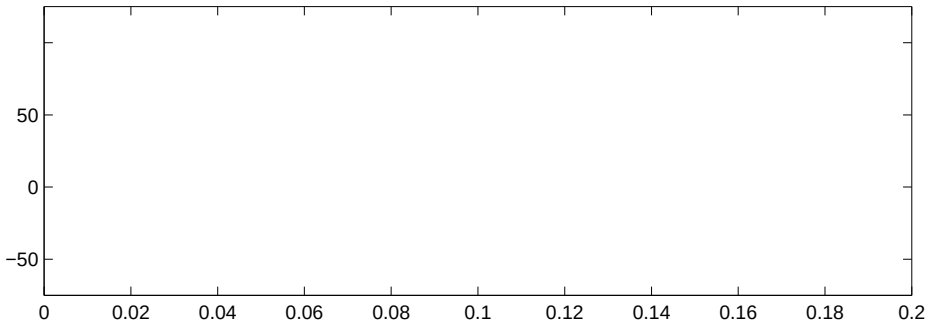
50
0
−50
0
0.02
0.04
0.06
0.08
0.1
0.12
0.14
0.16
0.18
0.2


0
0.02

8.3 Singulating parts with ramps

While the above waveforms result in part motion, nearby parts will tend to move as a group

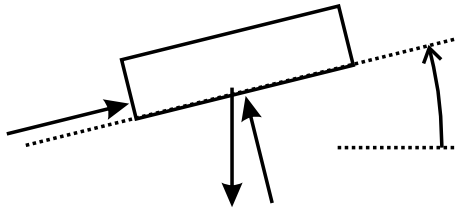

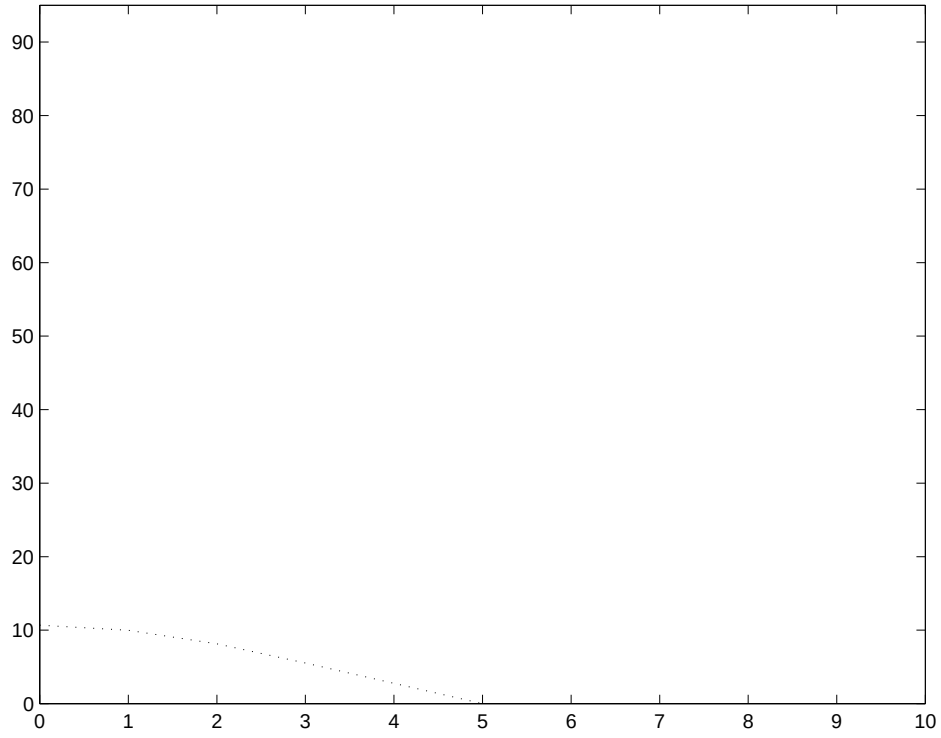
90
80
70
60
50
40
30
20
10
0
0
1
2
3
4
5
6
7
8
9
10

at the beginning of this chapter. The feeder has an annular feed path so that a single rotational vibration waveform of the feeder will suffice

Chapter 9

Conclusions

9.1 Advantages of low-OF

9.3 Planar robot design

This dissertation documents the first uses of the planar robot designed at CMU. There are several design issues that were impossible to resolve except after developing and using the prototype systems. Although the experiments of this dissertation were not designed specifically to explore these issues, the work did yield insights that are useful for validating some of the design decisions ac[illegible]

may be required for a particular part, dimensions of the sub-assembl

Much of the work of this dissertation also applies to higher-DOF robots that use planar motor technology, such as the robotic positioning heads of the RobotWorld and Megamation workcells,

f

eferen e

[53] F. Jacobs, "High resolution piggyback linear motor design for pcacement systems and the like." U.S. Patent 5,126,648, June 30, 1992. Megamation Incorporated.

[54] L. M. Ccark, "Linear motor technology for SMD pcacement," in *5th International SAMPE Electronics conference*, (Los Angeles, CA), pp. 202–208, June 1991.

[55] B. D. Hoffman, "The use of 2-D linear motors in surface mount technology," in *Proc. 5th Int'*

[66] A. A. Rizzi, J. Gowdy, and R. L. Hollis, "Agile assembly architecture: an agent based approach to modular precision manufacturing systems,"

[117] I. Kolmanovsky, E. G. Gilbert, N. H. McClamroch, and T. L. Maizenberg, “

Appendix

without violating the constraint combination j. Otherwise, the wrench output can-

The normal to the hyperplane can then be computed as

$$w_{N,j} = \left(I - d'_1 d'^T_1 \right.$$

A.2 Extension for time-varying controller terms

Assume a controller command

$$u_w = w_s(q,$$

$$
\begin{array}{cc}
i & p'^{T}_{\mathcal{V}_i} \\
1 & \left[\begin{array}{ccc} \frac{1}{\left(f_1^+ + f_2^+ + D_1^+\right)} & 0 & 0 \end{array}\right] \\
2 & \left[\begin{array}{ccc} \frac{1}{\left(f_1^- + f_2^- - D_1^-\right)} & 0 & 0 \end{array}\right] \\
3 & \left[\begin{array}{ccc} \frac{1}{2f_1^+ + 2f_3^+ - D_1^+ - D_2^+ + D_3^- / d_a} & \frac{1}{2f_1^+ + 2f_3^+ - D_1^+ - D_2^+ + D_3^- / d_a} & \frac{-1}{d_a(2f_1^+ + 2f_3^+ - D_1^+ - D_2^+ + D_3^- / d_a)} \end{array}\right] \\
4 & \left[\begin{array}{ccc} \frac{1}{2f_2^- - 2f_3^+ - D_1^- + D_2^+ - D_3^- / d_a} & \frac{-1}{2f_2^- - 2f_3^+ - D_1^- + D_2^+ - D_3^- / d_a} & \frac{1}{d_a(2f_2^- - 2f_3^+ - D_1^- + D_2^+ - D_3^- / d_a)} \end{array}\right] \\
5 & \left[\begin{array}{ccc} \frac{1}{2f_1^- + 2f_3^- - D_1^- - D_2^- + D_3^+ / d_a} & \frac{1}{2f_1^- + 2f_3^- - D_1^- - D_2^- + D_3^+ / d_a} & \frac{-1}{d_a(2f_1^- + 2f_3^- - D_1^- - D_2^- + D_3^+ / d_a} \end{array}\right. \\
6 & \left[\begin{array}{ccc} \frac{1}{2f_2^+ - 2f_3^- - D_1^+ + D_2^- - D_3^+ / d_a} & \frac{1 \quad -1}{2f_2^+ - 2f_3^- - D_1^+ + D_2^- - D_3^+ / d_a} & \frac{1}{d_a(2f_2^+ - 2f_3^- - D_1^+ + D_2^- - D_3^+ / d_a} \end{array}\right. \\
7 & \left[\begin{array}{ccc} \frac{1}{2f_1^- - 2f_4^+ - D_1^- + D_2^+ + D_3^+ / d_a} & \frac{1 \quad -1}{2f_1^- - 2f_4^+ - D_1^- + D_2^+ + D_3^+ / d_a} & \frac{-1}{d_a(2f_1^- - 2f_4^+ - D_1^- + D_2^+ + D_3^+ / d_a} \end{array}\right. \\
8 & \left[\begin{array}{ccc} \frac{1}{2f_2^+ + 2f_4^+ - D_1^+ - D_2^+ - D_3^+ / d_a} & \frac{1 \quad 1}{} & \end{array}\right.
\end{array}
$$

Appendix B

Stability domain for PD controller

Assume a Lyapunov candidate function

$$\eta = {}^{1}$$

positive, respectively. __ negative k_a value indicates an invalid design (*i.e.* the chosen controller gains are too high or $q_{\theta,max}$ is too big for the given physical parameters).

Proposition 4 *The time derivative of* $\frac{d}{dt}\frac{\hat{v}\hat{v}^T}{\hat{v}^T\hat{v}}$ *is* $\frac{D\hat{v}\dot{\hat{x}}\hat{v}^T}{\hat{v}^T\hat{v}} + \frac{\hat{v}\dot{\hat{x}}^T D\hat{v}}{\hat{v}^T\hat{v}} - \frac{2(\hat{v}^T D\hat{v}\dot{\hat{x}})(\hat{v}\hat{v}^T)}{(\hat{v}^T\hat{v})^2}$.

Begin by using the quotient rule, then simplify

$$\begin{aligned}
\tfrac{d}{dt}\tfrac{\hat{v}\hat{v}^T}{\hat{v}^T\hat{v}} &= \tfrac{\frac{d}{dt}(\hat{v}\hat{v}^T)(\hat{v}^T\hat{v}) - \frac{d}{dt}(\hat{v}^T\hat{v})(\hat{v}\hat{v}^T)}{(\hat{v}^T\hat{v})^2} \\
&= \tfrac{(D\hat{v}\dot{\hat{q}}\hat{v}^T + \hat{v}(D\hat{v}\dot{\hat{q}})^T)(\hat{v}^T\hat{v}) - ((D\hat{v}\dot{\hat{q}})^T\hat{v} + \hat{v}^T D\hat{v}\dot{\hat{q}})(\hat{v}\hat{v}^T)}{(\hat{v}^T\hat{v})^2} \\
&= \tfrac{(D\hat{v}\dot{\hat{q}}\hat{v}^T + \hat{v}\dot{\hat{q}}^T D\hat{v})(\hat{v}^T\hat{v}) - (2\hat{v}^T D\hat{v}\dot{\hat{q}})(\hat{v}\hat{v}^T)}{(\hat{v}^T\hat{v})^2} \\
&= \tfrac{D\hat{v}\dot{\hat{q}}\hat{v}^T}{\hat{v}^T\hat{v}} + \tfrac{\hat{v}\dot{\hat{q}}^T D\hat{v}}{\hat{v}^T\hat{v}} - \tfrac{2(\hat{v}^T D\hat{v}\dot{\hat{q}})(\hat{v}\hat{v}^T)}{(\hat{v}^T\hat{v})^2}.
\end{aligned} \tag{C.6}$$